Contents lists available at ScienceDirect

Materials Today Bio

journal homepage: www.journals.elsevier.com/materials-today-bio

Treatment with FAP-targeted zinc ferrite nanoparticles for rheumatoid arthritis by inducing endoplasmic reticulum stress and mitochondrial damage

Weizhong Qi [a,c,1], Li Jin [b,1], Cuixi Wu [a], Hao Liao [c], Mengdi Zhang [a], Zhaohua Zhu [a], Weiyu Han [a,c], Qiyue Chen [d,**], Changhai Ding [a,e,*]

[a] Clinical Research Centre, Zhujiang Hospital, Southern Medical University, Guangzhou, 510282, China
[b] Rheumatology and Clinical Immunology, ZhuJiang Hospital, Southern Medical University, Guangzhou, 510282, China
[c] Centre of Orthopedics, Zhujiang Hospital, Southern Medical University, Guangzhou, 510282, China
[d] Stomatological Hospital, Southern Medical University, Guangzhou, 510282, China
[e] Menzies Institute for Medical Research, University of Tasmania, 7000, Hobart, Tasmania, Australia

ARTICLE INFO

ABSTRACT

Rheumatoid arthritis (RA) is a common chronic inflammatory disease characterized by the proliferation of fibroblast-like synoviocytes (FLS), pannus development, cartilage, and bone degradation, and, eventually, loss of joint function. Fibroblast activating protein (FAP) is a particular product of activated FLS and is highly prevalent in RA-derived fibroblast-like synoviocytes (RA-FLS). In this study, zinc ferrite nanoparticles (ZF-NPs) were engineered to target FAP^+ (FAP positive) FLS. ZF-NPswere discovered to better target FAP^+ FLS due to the surface alteration of FAP peptide and to enhance RA-FLS apoptosis by activating the endoplasmic reticulum stress (ERS) system via the PERK-ATF4-CHOP, IRE1-XBP1 pathway, and mitochondrial damage of RA-FLS. Treatment with ZF-NPs under the influence of an alternating magnetic field (AMF) can significantly amplify ERS and mitochondrial damage via the magnetocaloric effect. It was also observed in adjuvant-induced arthritis (AIA) mice that FAP-targeted ZF-NPs (FAP-ZF-NPs) could significantly suppress synovitis *in vivo*, inhibit synovial tissue angiogenesis, protect articular cartilage, and reduce M1 macrophage infiltration in synovium in AIA mice. Furthermore, treatment of AIA mice with FAP-ZF-NPs was found to be more promising in the presence of an AMF. These findings demonstrate the potential utility of FAP-ZF-NPs in the treatment of RA.

1. Introduction

Rheumatoid arthritis (RA) is a prevalent chronic autoimmune disease. Its primary clinical manifestations include synovitis, pannus formation, cartilage and bone injury, and, ultimately, joint deformity and function loss [1,2]. Currently, nonsteroidal anti-inflammatory drugs, glucocorticoids, and anti-rheumatic drugs are used clinically to treat RA and improve patients' conditions [3,4]. Although these drugs can improve their quality of life by alleviating symptoms patients frequently experience adverse reactions after long-term use, including gastrointestinal disorder [5], infections [6], and cardiovascular complications [7]. Despite an abundance of drugs and treatment methods for RA, there is a dearth of effective therapies with minimal adverse effects. Therefore, further research is required to develop new treatment strategies for RA.

In recent years, the rapid development of nanomaterials and nanomedicine has enabled the introduction of novel therapeutic strategies for the treatment of a variety of diseases. Many technologies have been integrated in this interdisciplinary field, including microfluidic [8–10],

three-dimensional (3D) printing [11], pharmaceutical drugs [12,13], medical diagnosis and treatment [14], regenerative medicine and reproductive medicine [15,16] and so on. Due to their small size effect, surface effect, quantum effect, and other factors, nanomaterials exhibit a series of unique electromagnetic, optical, thermal, and mechanical properties in comparison to conventional materials [17]. These properties not only facilitate the development of new nanomaterials but also encourage future research and implementation of nanomaterial-based therapies in the treatment of RA [18]. ZF-NPs belong to the class of soft magnetic nanomaterials with excellent performance in biomedical applications [19]. It is widely employed in biomedical fields such as magnetic resonance imaging (MRI) [20], targeted drug delivery [21], and magnetic hyperthermia [22,23] due to its strong chemical stability, ease of manufacture, ease of modification, and enormous biological activity.

In healthy individuals, fibroblast-like synoviocytes (FLS) regulate normal leukocyte transport and joint homeostasis by nourishing the joint environment [24,25]. However, FLS frequently exhibits an aggressive and tumor-like character in RA [26]. The pathophysiological characteristics of RA-FLS are believed to be similar to those of cancer-associated fibroblasts (CAF), which contribute to tumor invasion and metastasis. Fibroblast activating protein (FAP), one of the primary indicators of CAF, is important in the pathophysiology of invasive tumors [24,27], and its expression in RA has been reported in the literature [28]. Furthermore, it was discovered that FAP overexpression in RA-FLS is associated with the invasive phenotype of FLS. This is accompanied by FLS enhanced proliferation and consequent RA cartilage degradation [29,30]. Therefore, directly triggering the death of FAP$^+$ FLS or limiting the interaction of FAP$^+$ FLS with other cells may be a promising strategy for RA treatment.

In this study, the FAP peptide was modified to achieve active targeting of invasive FLS, and the therapeutic potential of ZF-NPs in the context of RA was investigated. Following biochemical and biophysical validation of nanomaterials, the targeting and therapeutic effects of FAP peptide-modified ZF-NPs (FAP-ZF-NPs) under the action of AMF were investigated in vitro and *in vivo*. FAP-ZF-NPs successfully activated the PERK-ATF4-CHOP and IRE1-XBP1 signaling pathways in RA-FLS, causing endoplasmic reticulum stress (ERS) and mitochondrial damage, which caused apoptosis, reduced synovial angiogenesis, protected articular cartilage, and had a significant inhibitory effect on RA synovitis (Scheme 1). Finally, FAP-ZF-NPs were administered intra-articularly and tested *in vivo* for safety and potential therapeutic effects. This study demonstrates for the first time that FAP-ZF-NPs have the potential to be used to treat RA, revealing the untapped potential of nano drugs delivered using thermomagnetic for use in therapies that are efficient and comparatively safe.
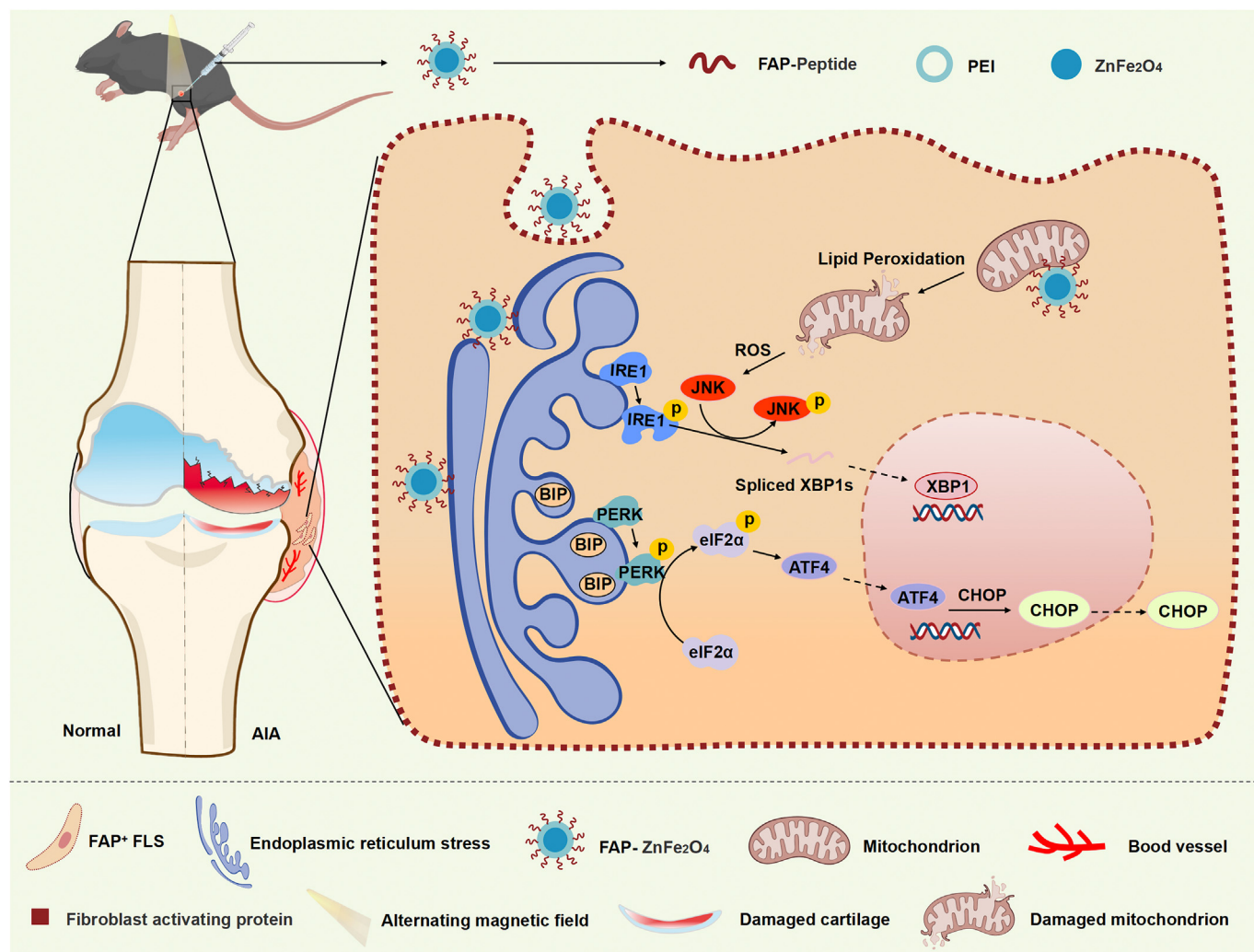
Scheme 1. Schematic illustration of the mechanism of action FAP-ZF-NPs in the treatment of RA. FAP-ZF-NPs can activate PERK-ATF4-CHOP and IRE1-XBP1 signaling pathways and promote ERS and mitochondrial damage in synovial FAP$^+$ cells under the influence of AMF, thereby inhibiting the process of synovitis.

2. Materials and methods

2.1. Preparation of ZF-NPs

ZF-NPs were prepared according to the previously reported synthesis method. Briefly, ferric nitrate and zinc nitrate solutions were mixed by metering followed by the addition of NaOH (2 M) to completely precipitate the metal ions. After that, the pH of the mixture was adjusted to 11–12 and the reaction temperature was set to 180 °C and allowed to incubate for 360 min. The resulting solution was then centrifuged and dialyzed and the product was isolated, filtered, and dried to yield ZF- NPs [23].

2.2. Preparation of ZF -NPs targeting FAP

After grafting ZF onto polyethyleneimine (PEI), 50 mg of ZF and 25 mg of PEI were completely dissolved in 50 mL of ultrapure water using ultrasonic stirring. After stirring, the supernatant was removed and the mixture was rinsed with ultrapure water. The PEI-ZF binding was produced by heating in an oven overnight. To prepare FAP-PEI-ZF, 30 mg FAP polypeptide, 1-Ethyl-3-[3-dimethylaminopropyl]-carbodiimide hydrochloride (EDC) and N- hydroxysuccinimide NHS (molar mass ratio with polypeptide is 1:1) were transferred into the 100 mL ultrapure water and stirred to activate carboxyl. After that, 20 mg PEI-ZF (mass ratio of PEI-ZF: polypeptide of 5:1) was incorporated into the above reaction mixture and incubated overnight in the dark at 4 °C. The resulting mixture was centrifuged and the obtained pellet was resuspended with ultrapure water.

2.3. Characterization of ZF nanoparticles

The morphology and size of nanoparticles were examined using high-resolution transmission electron microscopy (HRTEM) (FEI(G2 F30), USA) and dynamic light scattering (DLS)(USA, nanosizer 90). X-ray diffraction (XRD) (Smartlab, Japan) was used to examine the crystal structures of ZF-NPs and FAP-ZF-NPs. Changes in zeta potential (nanosizer 90, USA), Fourier Transform Infrared (FTIR) spectra (Horiba xlupa, Japan), and Ultraviolet–Visible Absorption (Horiba xlupa, Japan) spectra of ZF-NPs before and after FAP binding were examined using standard procedures. FAP-ZF-NPs were dispersed ultrasonically in deionized water (1 mg/mL) and transferred into a 1.5 mL plastic centrifuge tube. The centrifuge tube was exposed to an AMF (1.7 mT) for 5 min, and a forward-looking infrared (FLIR T420, USA) thermal imaging camera was used to record the temperature change of the solution at different time points in real-time and to draw a post hoc photothermal temperature rise curve.

2.4. Human samples

Tissue samples were collected from 10 RA patients. The diagnostic criteria for RA were revised in 1987 by the American College of Rheumatology. Patients with RA were included in the study, but those with malignant tumors, metabolic diseases, mental and neurological problems, and other immune system diseases were excluded. Specifically, samples from RA patients (n = 5; 65.4 ± 2.3 years of age; one male and four females) and osteoarthritis patients (n = 5; 68.3 ± 5.2 years of age; one male and four females) were included as controls in our dataset. Human specimens were collected from Zhujiang Hospital, with the approval of the Ethics Committee of Zhujiang Hospital, Southern Medical University, Guangzhou, China, (NO 2022-KY- 165-02). Each participant submitted their informed consent.

2.5. Animal modeling and treatment

The project aims to develop an adjuvant-induced arthritis (AIA) mouse model to simulate RA in the laboratory. Male C57/BL6 mice (8

weeks old, weight 20 ± 1.3g) were purchased from the Guangdong Experimental Animal Center (Guangzhou, Guangdong Province, P.R. China). The mice were fixed in position using a mouse fixator after being thoroughly sedated with isoflurane via inhalation. To elicit initial immunization, complete Freund's adjuvant was subcutaneously injected into the flank and groin skin on day 0. To produce delayed hypersensitivity, an incomplete Freund's adjuvant was injected into the knee joint cavity on day 7. On day 21, mice in the RA and treatment groups received an intra-articular injection of FAP-ZF-NPs (20 μg/mL, 5 μl) or were subjected to treatment with AMF. Thermal images of the mice's joints were obtained in separate treatment groups using an infrared thermal imager (FLIR T420, USA). The animal study was carried out in accordance with the Committee on Animal Care and Use guidelines (NO. LAEC-2021-129) and was reviewed and approved by the Ethics Committee of the Zhujiang Hospital, Southern Medical University.

2.6. Treatment of AIA mice with FAP-ZF-NPs

The AIA mouse model was developed to evaluate the *in vivo* therapeutic effects of ZF-NPs on AIA. AIA mice were randomly divided into four treatment groups (n = 6 for each group) two weeks after model establishment: (1) control group, (2) AMF group, (3) FAP-ZF-NPs group (the concentration of nanomaterials was 20 μg/mL, 5 μl in total), (4) FAP-ZF-NPs group + AMF group (the nanomaterials were injected into the articular cavity of mice, and mice were placed in the AMF setting the next day). Injections were administered to the mice once a week. Mice in the control group were injected with normal saline. Mice were sacrificed after 4 weeks of treatment, and their serum, knee joint, and visceral tissues were collected.

2.7. Biosafety evaluation of NPs on AIA mice

The purpose of this study is to examine the effects of various treatments on the weight changes and various physiological indicators of animals. Our specific objectives include weighing mice before and after therapy, collecting mouse serum, and performing blood biochemical testing. The hearts, spleen, lungs, liver, and kidneys of mice were also collected for hematoxylin-eosin (H&E) staining. The observations are expected to include the state of the outer membrane of the heart and myocardial cells, the cellular status of liver cells and hepatic portal area in liver tissue, the state of the splenic capsule and medullary area, morphological changes of the airway epithelium and alveoli in lung tissue, and cellular status of renal medulla and renal cortex. These observations will provide valuable insights into the effects of the various treatments on the physiological functions of the animals.

2.8. Assessment of arthritis severity

Histological sections were graded from 0 to 3 for each of the following five parameters: synovite (defined as synovial hypercellularity), exudate of joint space (defined as leucocytes in joint space), soft tissue inflammation (defined as leukocytes infiltration in the subpatellar adipose pads, the joint capsule and the area adjacent to the periosteal sheath), cartilage degradation (defined as loss of hematoxylin and eosin staining; 0 = stained cartilage, 3 = non stained cartilage) bone lesions (defined based on the extent and depth of subchondrial bone lesions). The sum of each observable characteristic (up to a maximum of 15) produced the total histology result [31].

2.9. Tissue section staining

Sections with a thickness of 5 μm were formed after drying human and animal tissue specimens and forming wax blocks. Deparaffinization was performed in xylene, followed by rehydration through a gradient of decreasing ethanol concentration. The sections were then stained with toluidine blue (TB)(Solarbio, China) and H&E for histological

investigation. Following staining, the samples were examined and photographed under a microscope, followed by statistical analysis.

2.10. Cell culture and treatments

Both normal FLS and RA-FLS were purchased from Cell Applications, Inc (San Diego, CA, USA) and cultured in Dulbecco's Modified Eagle Medium (DMEM) medium supplemented with 5% FBS and penicillin (100 U/mL), and 100 mg/mL streptomycin sulfate (Life Technologies, USA) at 37 °C with 5% CO2. The cells were then treated for 24 h with varying amounts of FAP-ZF-NPs, ZF-NPs, or the endoplasmic reticulum stress activator thapsigargin.

2.11. Cell migration

In a 24-well plate, 1.5×10^5 cells were added. After the cell fusion rate reached 95% or higher, a pipette tip perpendicular to the cell surface was used to scratch the cells. After that, the cells were washed with sterile PBS to remove any detached cells from the scratch line, then transferred to the serum-free culture medium and subjected to incubation at 37 °C in an incubator with 5% CO_2. The cells were cultured for 24 h before being removed from the plate and photographed under a microscope followed by the determination of scratch density.

2.12. Transwell assay

FAP-ZF-NPs treated cells were suspended in a low serum (5% FBS) medium and seeded into the upper chamber of the transwell with a filter. The lower chamber was filled with complete medium (including 10% FBS). Migrating cells on the bottom surface were stained with 0.5% crystal violet after 12 h.

2.13. EdU labeling and staining

The treated cells were also subjected to formaldehyde fixation. Following that, a 5-ethynyl-2′-deoxyuridine (EdU) reaction mixture was prepared and the cells were incubated in the dark for 30 min. The nuclei were counterstained with Hoechst and photographed using a microscope.

2.14. Lipid peroxidation and JC-1 detection

®Lipid Peroxidation Assay Kit (Invitrogen, USA) and Mitochondrial Membrane Potential Assay Kit (Solarbio, China) were used to examine the influence of ZF-NPs on lipid peroxidation and mitochondrial potential in cells.

2.15. Western blot

Lysis buffer was used to lyse treated cells. Samples with identical levels of total protein were evaluated and then transferred after that, analyzed with the imaging system after electrophoretic transfer. The following antibodies were applied: anti-BIP (CST, C50B12), anti-CHOP (CST, L63F7), anti-p-PERK CST, D11A8), anti-PERK (CST, 16F8), anti-eIF2α (CST, D7D3), anti-p-eIF2α (CST, D9G8), anti-ATF4 (proteintech, 10835-1-AP), anti-Ero1-Lα(CST, 3264T), anti-Cyt C (proteintech, 10993-1-AP), anti-JNK (CST, 9252T), anti-p-JNK (CST, 9251S), anti-XBP1s (CST, E9V3E), anti-IRE1α (CST, 3294T), anti-p-IRE1α (Abcam, ab124945).

2.16. Immunohistochemistry and immunofluorescence

Immunostaining was performed as directed by the manufacturer. The following antibodies were utilized: anti-F4/80 (Abcam, ab6640), anti-iNOS (proteintech, 80517- 1-RR), anti-CD31 (Santa Cruz, sc-376764), anti-FAP (Bioss, bs-34078R), anti-COL II (Abcam, ab34712), anti-

VIMENTIN (Santa Cruz, sc-6260), anti-CD206 (Abcam, ab64693). Alexa 594 or 488 dye-labeled secondary antibodies (Jackson ImmunoResearch 383 Laboratories, Inc.) followed by overnight incubation at 4 °C.

2.17. Statistical analysis

All values were expressed as mean standard deviation (SD), and the data were analyzed with GraphPad Prism using either the Student t-test or an ANOVA. The Pearson correlation coefficient was used to calculate the correlation variables between the two approaches, and statistical significance was established at $P < 0.05$.

3. Results and discussion

3.1. FAP^+ FLS are increased significantly during the synovitis process

In RA, FLS exhibit an altered and aggressive character, which is important for disease progression, FLS recruitment to inflammatory sites, and articular cartilage and bone degradation [32,33]. Because of the similarity between RA-FLS and cancer cells, synovial tumor-like expansion can occur, resulting in an expanded local vascular network of rapid proliferation, apoptosis escape, and high production of growth and angiogenic factors. To investigate the role of synovial invasive lesions in RA, synovial hyperplasia and synovial angiogenesis were first studied in the synovial tissue of patients with RA. Similar to previous studies, H&E staining of the synovial tissue of RA patients revealed high levels of synovial hyperplasia and angiogenesis as well as abundant cell infiltration.

Articular cartilage tissue from RA patients was mildly stained with TB staining, indicating different degrees of erosion and degradation (Fig. 1A). H&E examination of extracted samples revealed varying degrees of proliferation in the synovial tissue of the knee joint of AIA mice six weeks after following the development of the AIA animal model. Moreover, TB staining revealed the mild staining of articular cartilage (Fig. 1F). The immunohistochemical staining of COL II (a cartilage marker) revealed a low expression of this protein in the cartilage tissue of RA patients (Fig. 1B) and AIA mice (Fig. 1G). Immunohistochemical staining confirmed the higher number of CD31-positive cells in synovial tissues of patients with RA (Fig. 1C) and AIA mice (Fig. 1H) upon comparison with controls, suggesting that patients with RA and AIA mice have increased synovial angiogenesis. Furthermore, immunohistochemical staining revealed that the positive staining of FAP was dramatically enhanced in synovial tissues from RA patients (Fig. 1D) and AIA mice (Fig. 1I). Double staining of FAP and VIMENTIN (synovial cell marker) revealed that FAP^+ FLS increased in the synovial tissue, confirming the expression and localization of FAP in synovial tissues. Overall, these findings demonstrated that FAP was activated in the FLS of both RA patients (Fig. 1E) and AIA mice (Fig. 1J).

3.2. Characterization of FAP-targeted ZF-NPs

As previously described, FAP^+ FLS were significantly increased during the development of RA. Therefore, a therapeutic approach focused on hindering FAP^+ FLS pathways is critical for the treatment of RA. Previous studies have reported that ZF-NPs can not only be used as a mediator of magnetic hyperthermia, but they can also alter the cellular state. Therefore, a specific binding target peptide was used in this study to achieve a targeted strategy of ZF-NPs to FAP^+ FLS. Initially, ZF-NPs were synthesized based on previous research and experimental protocols.

ZF-NPs were selected as precursors in this study. The element distribution of the surface of ZF-NPs was analyzed by element mapping and the results demonstrated the uniform distribution of zinc, iron, and oxygen on the surface of ZF-NPs as shown in Fig. 2A. TEM and DLS techniques were utilized to detect FAP-ZF-NPs and evaluate their appearance and size. The FAP peptide was found on the surface of the ZF-NPs. SEM
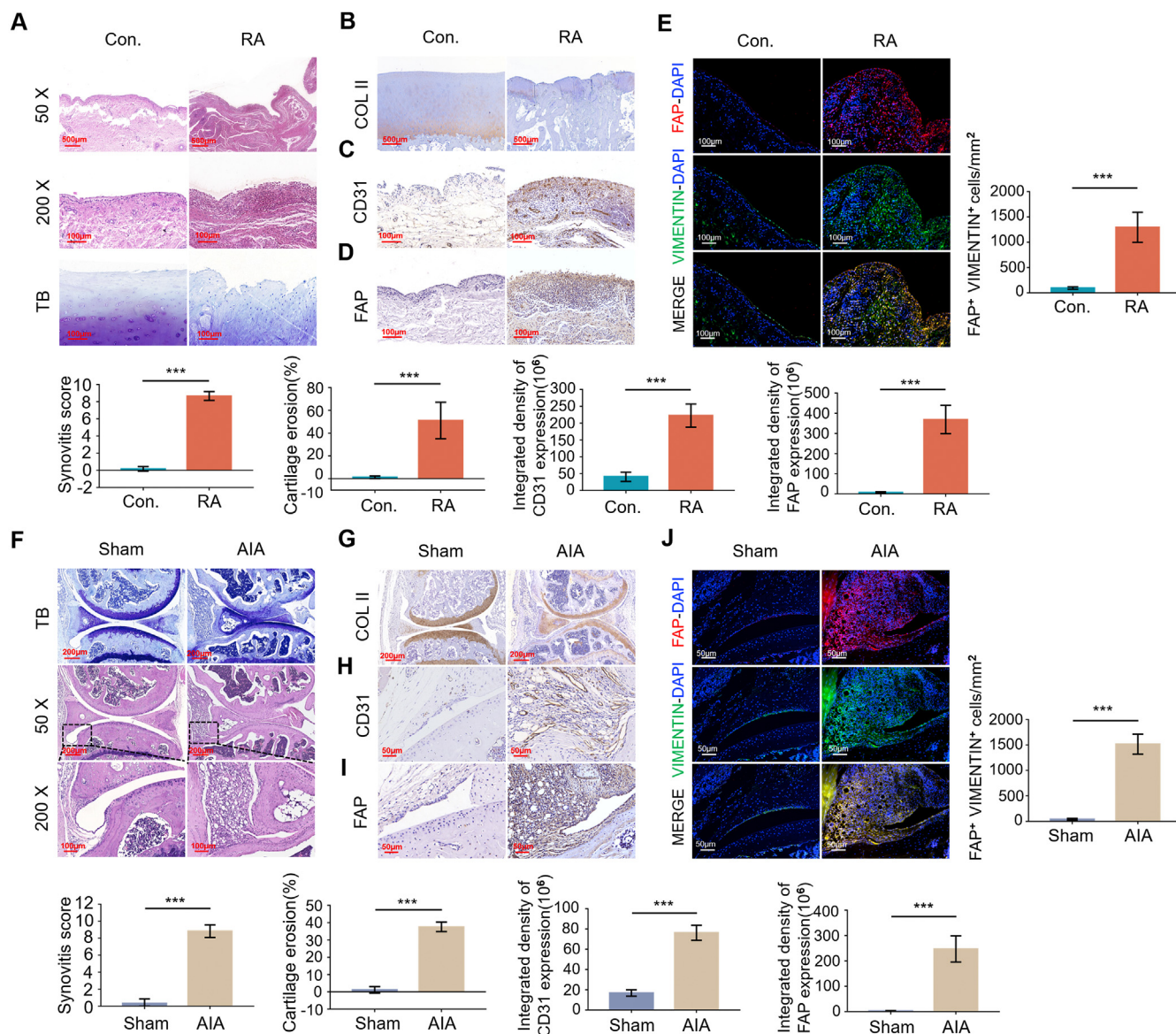
Fig. 1. FAP + FLS are increased significantly during the synovitis process (A) Representative images of H&E and TB staining in the synovial tissues of normal and RA patients (Scale bars, 100 μm or 500 μm). Immunohistochemistry based detection of the expression of COL II (B), CD31 (C), and FAP (D) in human synovial tissues (Scale bars, 100 μm or 500 μm). (E) Representative immunofluorescence images and quantitative analysis of VIMENTIN in FAP + cells in the synovial tissues of normal and RA patients (Scale bars, 100 μm). (F) Representative images of H&E and TB staining in the synovial tissues of AIA mice and sham groups (Scale bars, 100 μm or 200 μm). (B) Expression of COL II (G), CD31 (H), and FAP (I) in mice synovial tissues detected via immunohistochemistry (Scale bars, 50 μm or 200 μm). (J) Representative immunofluorescence staining images and quantitative analysis of VIMENTIN in FAP + cells in the synovial tissues of AIA mice and sham groups (Scale bars, 50 μm). The data is presented as mean ± SD analyzed by one-way ANOVA. **P < 0.05, ***P < 0.01.

images revealed the good dispensability of the synthesized ZF-NPs (Fig. 2B). Following this, DLS was used to analyze the NP hydrate particle size of each sample of ZF-NPs in the solution (Fig. 2C). The average hydrodynamic diameter of FAP-ZF-NPs (71.83 ± 2.93 nm) was somewhat larger than that of ZF-NPs (31.32 ± 1.83 nm) due to the conjugation of targeted peptides on the surface of FAP-ZF-NPs material, indicating that the FAP was efficiently modified on the surface of ZF-NPs. Furthermore, when compared to ZF-NPs (10.52 ± 0.19 mV), the zeta potential of FAP-ZF-NPs increased to 20.93 ± 0.33 mV (Fig. 2D). Simultaneously, the combination of FAP peptide and ZF-NPs was investigated by UV FTIR (Fig. 2E) and UV (Fig. 2F). The FAP-ZF-NPs X-ray diffraction test data (Fig. 2G) was found to be similar to the ZF-NPs characteristic peak (Fig. 2H), suggesting that the grafted nanomaterial maintained its crystal structure and paving the way for magneto thermal

evaluation. Furthermore, the FAP peptide XRD test revealed that there was no obvious characteristic peak, despite the presence of a unique steamed bread peak structure that was consistent with the FAP peptide's properties.

3.3. Magnetocaloric characterization of FAP-targeted ZF-NPs and therapeutic model of AIA in mice

The FAP-ZF-NPs structure designed in this investigation consists of a ZF-NPs core and FAP-peptide-modified surface. Consequently, FAP-ZF-NPs should have the same magnetic and magnetothermal properties as ZF-NPs. These findings reveal no statistically significant differences between ZF-NPs and FAP-ZF-NPs. The increase in temperature of ZF-NPs and FAP-ZF-NPs over time was comparable, indicating that the
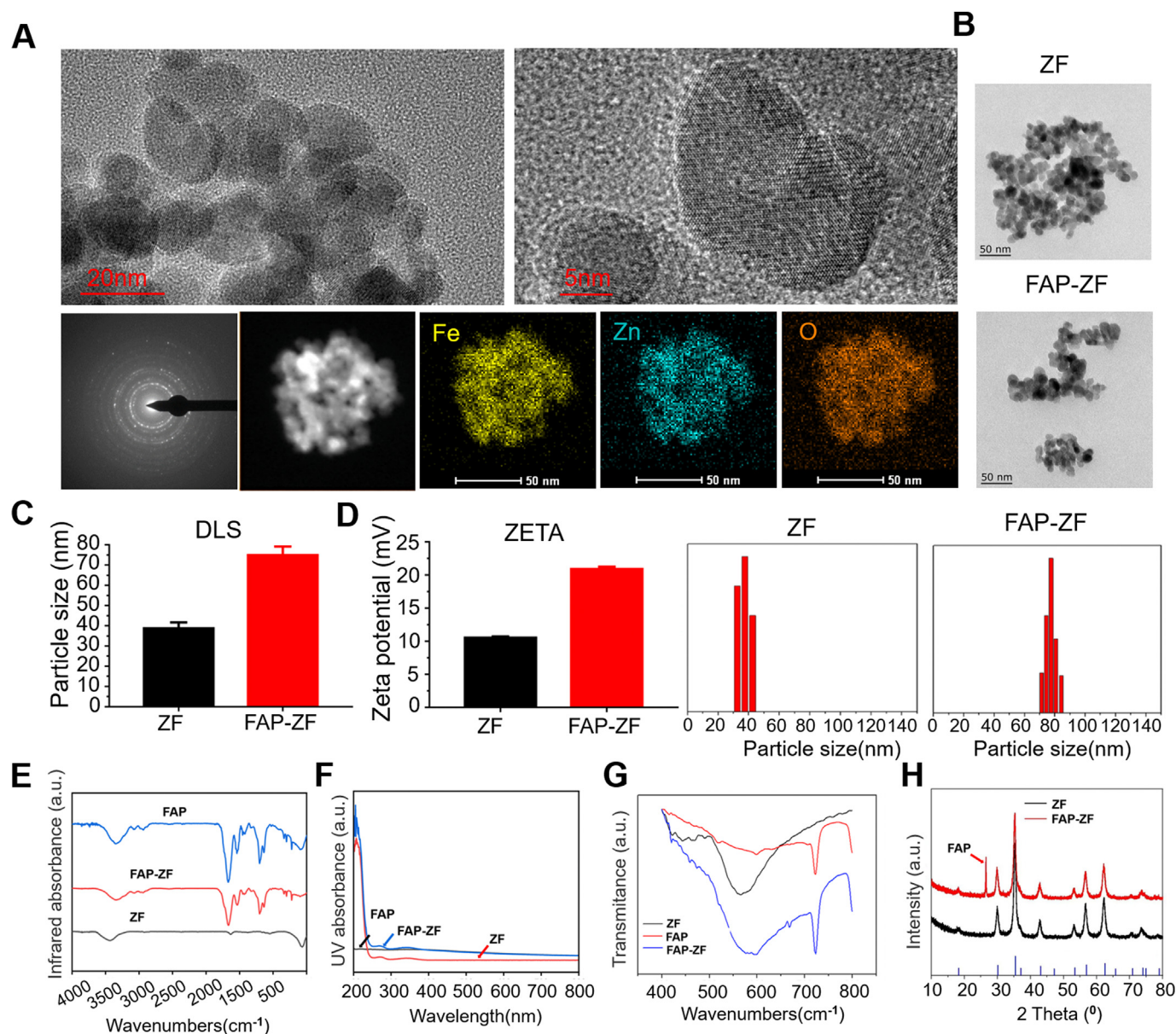
Fig. 2. Characterization of FAP-targeted ZF-NPs (A) TEM images and corresponding elemental mapping of ZF-NPs. (B) SEM images of ZF-NPs and FAP-ZF-NPs. (C) DLS analysis of ZF-NPs and FAP- ZF-NPs. (D) ZETA of ZF-NPs and FAP-ZF-NPs. (E) FTIR spectra of ZF-NPs and FAP-ZF-NPs. (F) UV–vis absorption spectra of ZF-NPs and FAP-ZF-NPs. (G) XRD patterns of ZF-NPs and FAP-ZF-NPs. (H) Characteristic peak of ZF-NPs and FAP-ZF-NPs.

modification of the FAP peptide did not substantially alter the magnetocaloric properties of ZF-NPs (Fig. 3A). Therefore, FAP-ZF-NPs are regarded as having a strong magnetocaloric effect.

The influence of magnetocaloric materials *in vivo* was further verified. Mice were injected with FAP-ZF-NPs into their joint cavity for these animal investigations and then placed in the AMF environment the next day to induce a magnetocaloric effect (Fig. 3B). An infrared camera was used to record temperature fluctuations in the knee joint. In comparison to the control group, the FAP-ZF-NPs group demonstrated a good magnetocaloric effect in the joint cavity of mice under the influence of AMF (Fig. 3C).

3.4. Effects of nanomaterials on synoviocytes

Previous research has shown that FAP expression levels in RA synovial tissue can be elevated. After extracting FLS from both normal and RA synovial tissue, it was discovered that FLS generated from RA synovial tissue expressed much more FAP than FLS obtained from normal synovial

tissue (Fig. 4A). This phenomenon is consistent with previous research and the design direction of this subject. The concentration of FAP-ZF-NPs was determined by adding FAP-ZF-NPs and ZF-NPs to RA-FLS and FLS, respectively. A CCK8 investigation confirmed the influence on cell viability and the CCK8 tests were used to measure cell growth rates in response to treatments. Various treatment concentrations (1, 2, 5, 10, 20, 40, 80, and 160 μg/ml) were initially administered to cell cultures. The experimental nanomaterials concentration was determined by selecting the lowest treatment concentration that resulted in a cell survival rate of 80% or higher. Finally, the treatment concentration ranges for FAP-ZF-NPs were adjusted to four appropriate concentrations. FAP-ZF-NPs-NPs (0, 10, 20, 40 μg/ml) were then delivered at the prescribed experimental treatment concentrations. In RA-FLS, the results indicated that FAP-ZF-NPs exhibited more inhibitory effect than ZF-NPs, and a concentration of 20 μg/ml was selected for the experiment. In FLS, ZF-NPs appeared to be more effective than FAP-ZF-NPs above 40 μg/ml, so a concentration of 20 μg/ml was selected for testing (Fig. 4B).

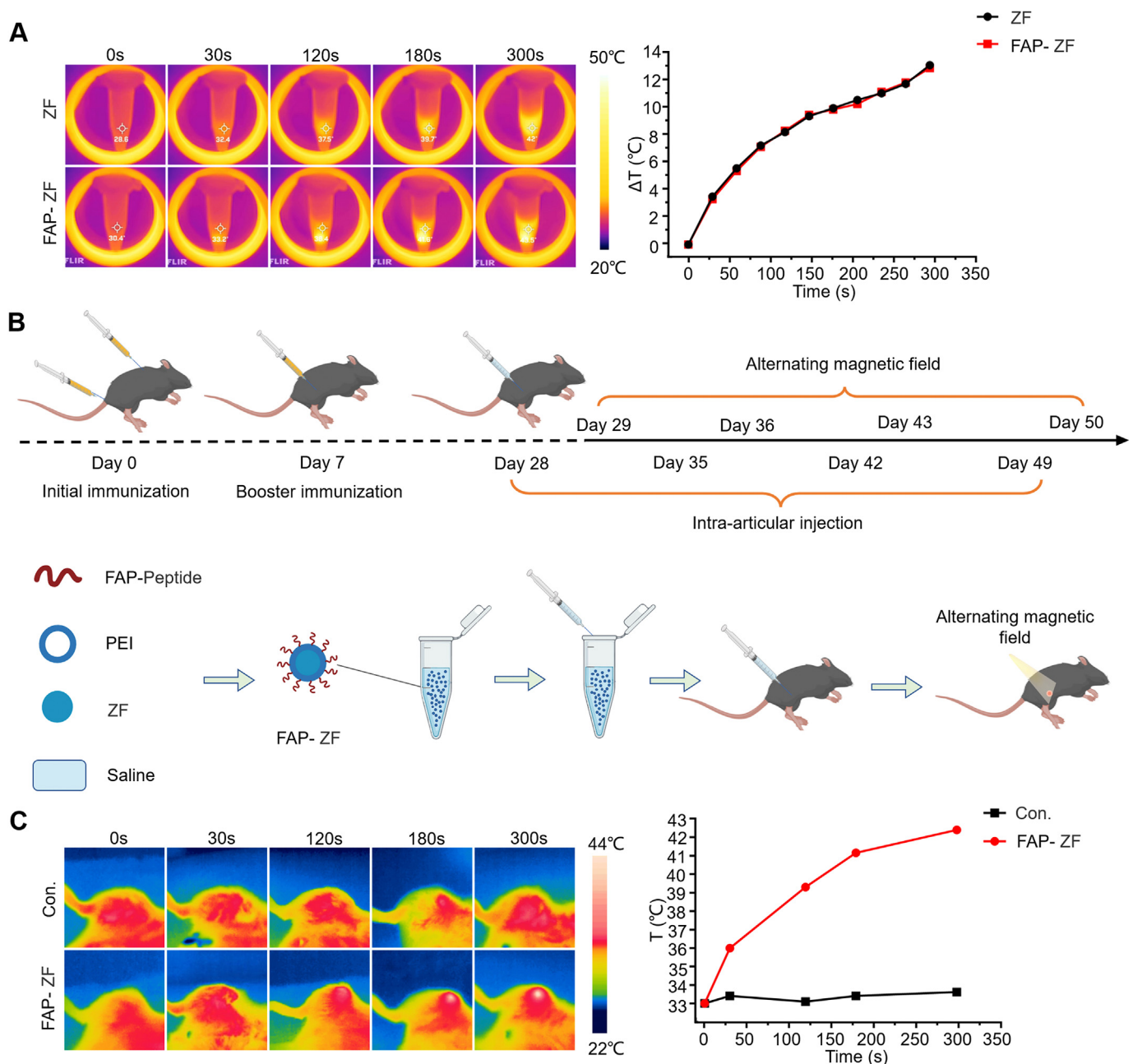After that, the targeting effect of these nanoparticles on FLS and RA-

Fig. 3. Magnetocaloric characterization of FAP-targeted ZF-NPs and therapeutic model of AIA in mice (A) Infrared images representing the temperature of nanomaterials heated by AMF. (B) Schematic illustration of the development of AIA mice model and treatment regimen. (C) Infrared images depicting mouse knee temperature after treatment.

FLS was evaluated by adding the fluorescent marker CYC5.5 to FAP-ZF-NPs. It was observed that the RA-FLS had a better uptake of FAP-ZF-NPs than FLS cells. RA-FLS were capable of adapting more FAP-ZF-NPs over time (Fig. 4C). This could be related to the more obvious targeting of FAP peptides. Fibroblast FAP is a membrane-bound protease that is currently under investigation as a target across multiple cancer types. This is due to its notably high levels in tumors juxtaposed with its limited expression in normal tissues. In our study, we observed high expression of FAP in pathogenic synovial cells, leading us to hypothesize that targeting FAP-positive synovial cells may yield beneficial effects in the treatment of synovitis. Positron Emission Tomography (PET) imaging that specifically targets FAP on the surface of cancer-associated fibroblasts has shown promising results in tumor diagnostics. FAP-2286, a FAP inhibitor, utilizes cyclic peptides as FAP-binding motifs to optimize tumor retention, demonstrating a superior performance compared to the small-molecule

FAP inhibitor series such as FAPI-04/46 [34,35].

Drawing from this body of research, we propose an innovative approach that involves grafting FAP-targeting peptide sequences onto nano zinc ferrite particles. The aim of this strategy is to imbue the nanoparticles with FAP-targeting capabilities, thereby enhancing their therapeutic impact on FAP^+ FLS. We believe that this targeted approach could offer a promising new avenue for the treatment of conditions characterized by high FAP expression.

To test the efficacy of FAP-ZF-NPs in RA-FLS, ZF-NPs were used as a control group. We added 20 μg/ml of FAP-ZF-NPs and ZF-NPs to RA-FLS, respectively, and the effect on cell migration was confirmed using a transwell assay. The inhibitory effect of FAP-ZF-NPs on the migration of RA-FLS was found to be greater than that of ZF-NPs at the same concentration. EdU labeling revealed that FAP-ZF-NPs had a greater proliferation of RA-FLS than the control group. FAP-ZF-NPs were discovered to
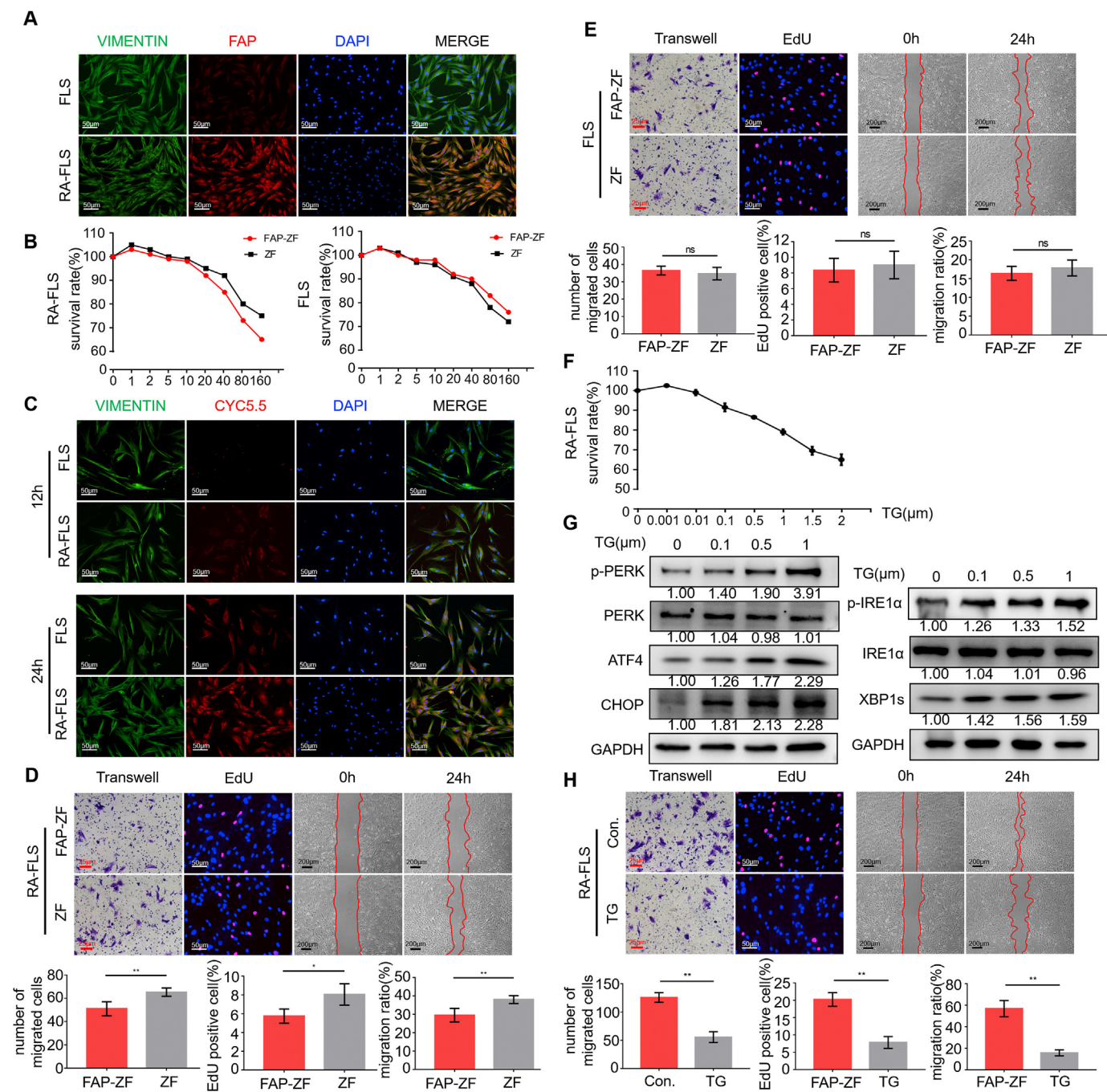
Fig. 4. The effects of nanomaterials on synoviocytes (A) The immunofluorescence images of FAP and VIMENTIN in FLS and RA-FLS. (B) The cell survival rate of the FLS and RA-FLS after the treatment of FAP-ZF-NPs and ZF-NPs at 12 h. (C) Immunofluorescence imaging of the FLS and RA-FLS after CFAP-ZF-NPs treatment at 12 h and 24 h. (D) Representative images of Transwell, EdU, and Wound-healing assay of RA-FLS after the treatment of FAP-ZF and ZF. (E) Representative images of Transwell, EdU, and Wound-healing assay of FLS after the treatment of FAP-ZF and ZF. (F) The cell survival rate of the RA-FLS after TG treatment at 12 h. (G)Western blotting analysis of endoplasmic reticulum stress pathway after TG treatment. (H) Representative images of Transwell, EdU, and Wound-healing assay of FLS after the treatment of TG. *P < 0.05, **P < 0.01.

have a more potent inhibitory effect on migration than ZF-NPs in the migration experiment suggesting that FAP-ZF-NPs have stronger inhibitory effects in RA-FLS compared with ZF-NPs (Fig. 4D). Simultaneously, FAP-ZF-NPs and ZF-NPs on ordinary FLS were also investigated. At a stimulation concentration of 20 μg/ml, transwell, EdU, and scratch experiments were carried out. No significant difference was observed between FAP-ZF-NPs and ZF-NPs in FLS. This may be associated with the fact that the FLS cells do not express FAP, hence exhibiting any significant difference in the uptake of FAP-ZF-NP and ZF-NP by FLS (Fig. 4E).

Previous research has demonstrated that endoplasmic reticulum

stress is an essential intracellular process. Various studies have demonstrated that ERS is a key mechanism of cell injury induced by both internal and external environmental factors [36–38]. Among these, thapsigargin (TG) has been identified as an activator that promotes endoplasmic reticulum stress. CCK8 was used to validate the concentration of TG for usage in RA-FLS. After 24 h of stimulation, doses with a survival rate exceeding 80% (0.1 μM, 0.5 μM, 1 μM) were selected as the subsequent experimental concentrations (Fig. 4F). A Western blot investigation revealed that TG can promote the RA-FLS endoplasmic reticulum stress state (Fig. 4G). Transwell, EdU, and scratch studies

revealed that TG could decrease RA-FLS migration and proliferation by inducing endoplasmic reticulum stress. Therefore, endoplasmic reticulum stress is thought to be one of the primary mechanisms for activating or inhibiting synovitis (Fig. 4H).

3.5. FAP-ZF-NPs can induce ERS and mitochondrial damage

The concentration of FAP-ZF employed on RA-FLS validated by the previous experiment section was selected as the succeeding experimental concentration under the condition of 24 h simulation (10, 20, 40 μg/ml) with a survival rate of more than 80%. After making FAP$^+$ RA-FLS more absorbable to FAP-ZF-NPs, the effect of FAP-ZF-NPs was verified on cell migration in vitro through a transwell assay. The results revealed that increasing FAP-ZF-NPs concentrations led to a significant decrease in the migration of RA-FLS (Fig. 5A). EdU labeling revealed that the proliferation of RA-FLS with FAP-ZF-NPs was significantly suppressed compared to the control group, whereas the suppression of RA-FLS proliferation was more pronounced at higher concentrations (Fig. 5B). Concerning the role of FAP-ZF-NPs in modulating RA-FLS migration, it was observed that the wound healing potential of RA-FLS decreased as FAP-ZF-NP concentrations increased. These results suggest that FAP-ZF-NPs incubation may influence the ability of RA-FLS to migrate in vitro (Fig. 5C).

In general, nanomaterials are found in the endoplasmic reticulum following endocytosis, where they may alter the milieu, interfering with the folding of synthetic proteins and causing ERS and unfolded protein response (UPR) [39]. Increased expression of these chaperones in the endoplasmic reticulum represents an internal marker of ERS and frequently indicates the presence of unfolded proteins in the endoplasmic reticulum [40]. In contrast, the expression of the marker protein eIF2α of the endoplasmic reticulum remained constant. Increased expression of both the PERK protein and its phosphorylated version was observed, indicating that FAP-ZF-NPs can activate the UPR's negative feedback regulatory pathway PERK. Furthermore, by examining the expression of proteins downstream of ERS induced by FAP-ZF-NPs in RA-FLS, it was found that ATF-4 and cytochrome c (Cyt C) levels were elevated in these cells. Among these, Cyt C is an intriguing marker because it is an essential protein present between the mitochondrial internal and exterior membranes. When cells are activated by apoptotic signals, mitochondria release Cyt C into the cytoplasmic matrix, triggering the formation of an apoptotic body and cellular apoptosis [41]. Interestingly, XBP1s, JNK, IRE1α protein, and phosphorylation levels were increased in the FAP-ZF-NPs group compared with the control group (Fig. 5D). This evidence suggests that FAP-ZF-NPs can activate IRE1α in RA-FLS cells and that FAP-ZF-NPs induce UPR via ERS, which leads to RA-FLS death.

Considering this information, Lipid Peroxidation Assay Kit was used to detect whether incubation with FAP-ZF-NPs induced free radical-
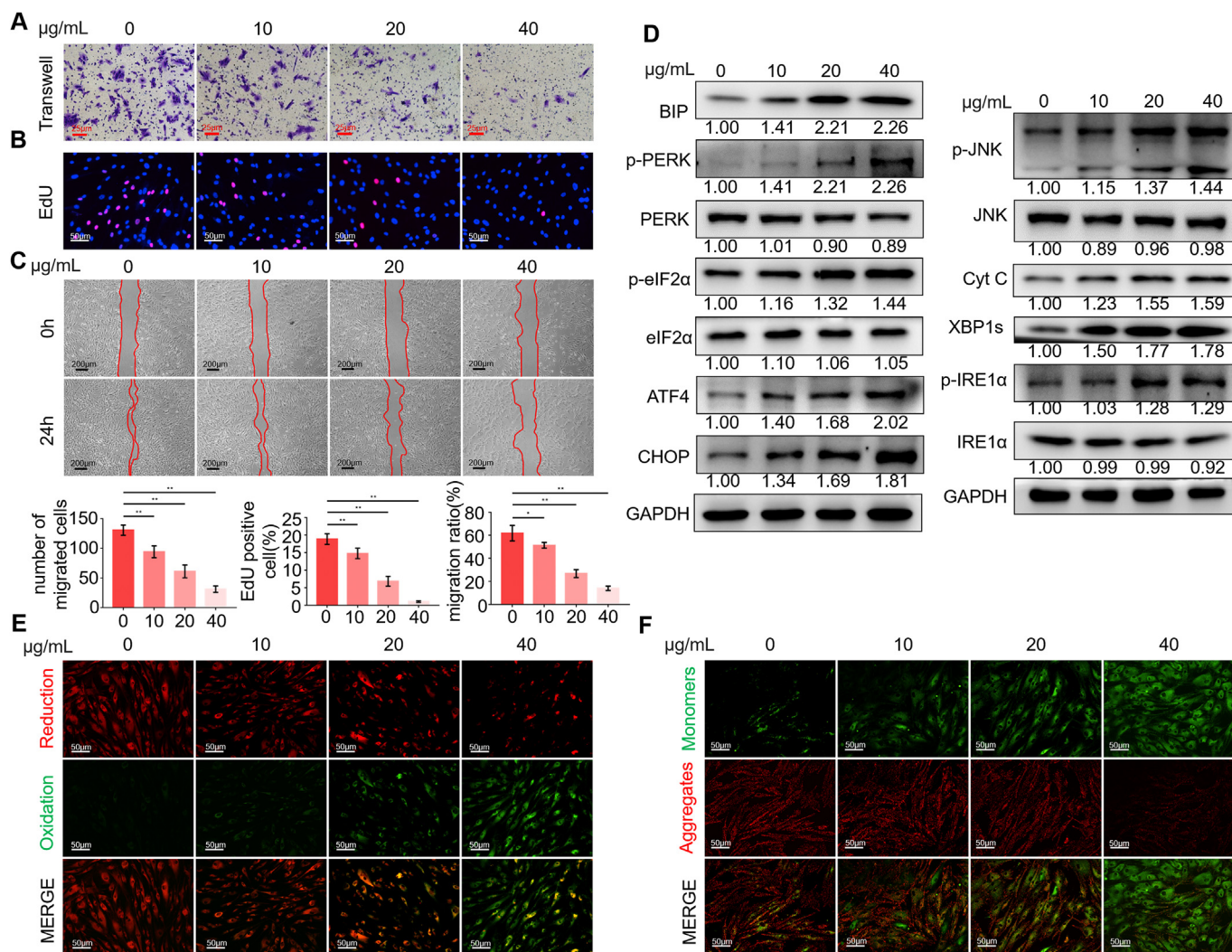

Fig. 5. FAP-ZF-NPs can induce ERS and mitochondrial damage (A) Representative images of transwell, (B) EdU, and (C) Wound-healing assay. (D) Western blotting analysis of endoplasmic reticulum stress pathway. (E) Representative images of lipid peroxidation and (F) mitochondrial membrane potential. **P < 0.05, ***P < 0.01.

mediated RA-FLS injury. FAP-ZF-NPs significantly accelerated the oxidative degradation of RA-FLS compared with the control group (Fig. 5E) suggesting that the FAP-ZF-NPs can significantly induce the production of reactive oxygen species (ROS) in RA-FLS. Apoptosis is characterized by a decrease in mitochondrial membrane potential, which is caused by mitochondrial damage [42]. Because of the high polarity of the potential of the mitochondrial membrane, normal cells can rapidly ingest a JC-1 probe into the mitochondria, forming clusters that exhibit red fluorescence at 488 nm excitation wavelength. JC-I probes frequently exist as monomers and produce green fluorescence after being excited at 543 nm, as a result of the reduced potential of the mitochondrial membrane in apoptotic cells. Mitochondrial membrane potential in FAP-ZF-NPs-treated cells was typically lower than in the control group. In conjunction with the apoptosis detection results, this suggests that FAP-ZF-NP induced decreased mitochondrial membrane potential and promoted apoptosis in RA-FLS cells (Fig. 5F). Overall, it was hypothesized that FAP-ZF-NPs can induce the PERK-ATF4-CHOP and IRE1-XBP1 pathways of ERS in RA-FLS cells, producing mitochondrial damage and inhibiting normal function.

3.6. Magnetothermal effect can potentiate ERS and mitochondrial damage induced by FAP- ZF-NPs

As previously stated, FAP-ZF-NPs is a ferrous material with a unique magnetocaloric effect. To further explore the magnetothermal effects of FAP-ZF-NPs on ERS and mitochondrial damage in RA-FLS, a 20 µg/ml concentration was selected as the experimental concentration to examine the changes in the state of RA-FLS, ERS, and mitochondrial damage under the influence of AMF.

Initially, cell morphology of migration (Fig. 6A), proliferation (Fig. 6B), and migration (Fig. 6C) were investigated. Cells in the AMF group were not inhibited as compared to the control group. Incubation with FAP-ZF-NPs was observed to significantly reduce AMF-induced migration, proliferation, and migration. The detection of ERS-related proteins by Western blot enabled us to determine that incubation with FAP-ZF-NPs causes an increase in BIP under AMF conditions, accompanied by a distinct ERS response. FAP-ZF-NPs exhibited an upregulation of UPR-related proteins PERK and eIF2α under the influence of AMF. In this regard, both the protein and its phosphorylated form increased,
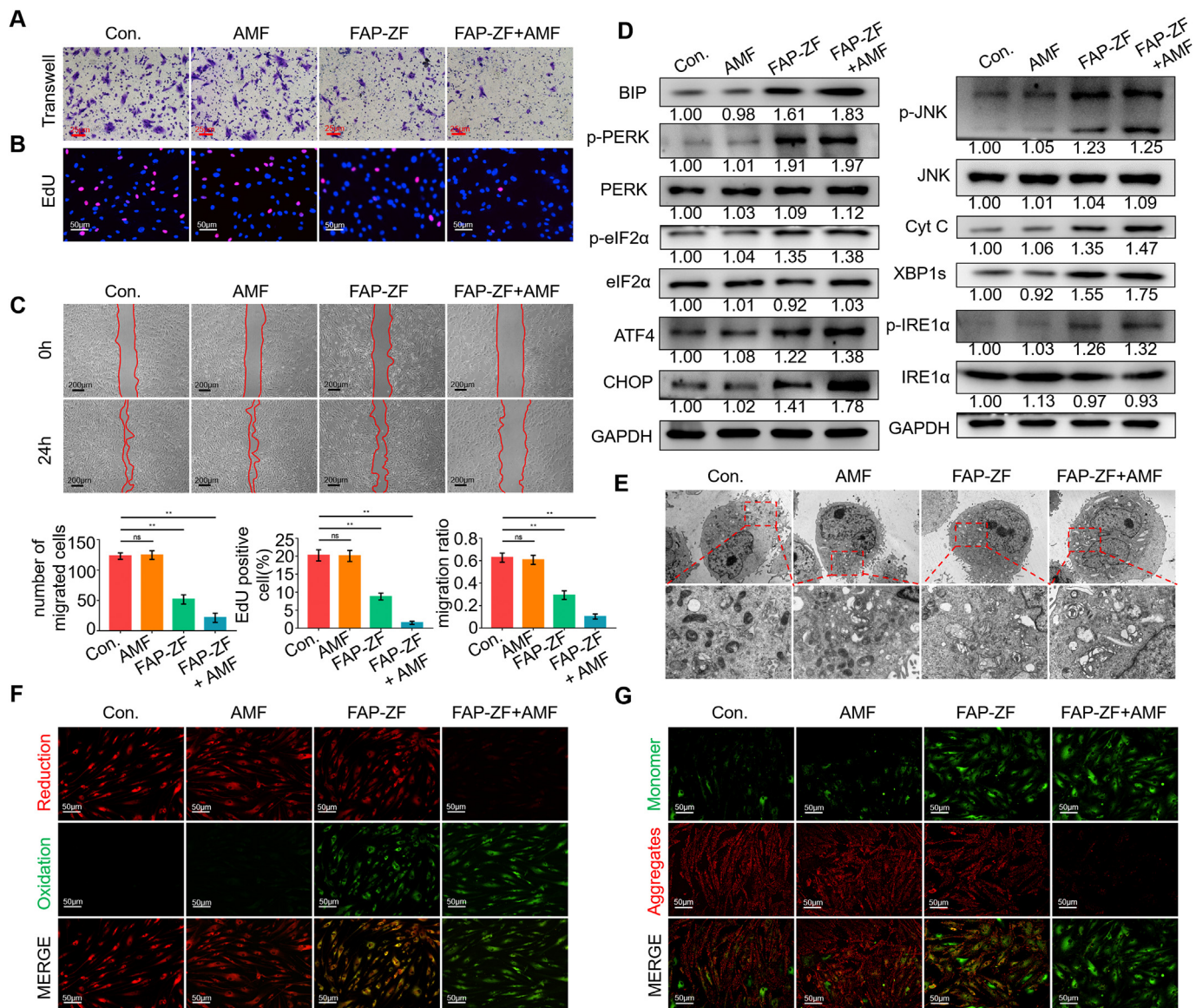

Fig. 6. Magnetothermal effect can potentiate ERS and mitochondrial damage induced by FAP-ZF-NPs Representative images of transwell, (B) EdU, and (C) Wound-healing assay. (D) Western blotting analysis of endoplasmic reticulum stress pathway. (E) The endoplasmic reticulum and mitochondria were detected by TEM. (F) Representative images of lipid peroxidation and (G) mitochondrial membrane potential. **P < 0.05, ***P < 0.01.

indicating that the magnetocaloric effect can substantially enhance the negative feedback regulatory pathway PERK pathway of FAP-ZF-NPs activating UPR (Fig. 6D). Similarly, ATF-4 and Cyt C proteins were significantly increased under AMF conditions. AMF significantly increased the JNK, IRE1, and XBP1s protein and phosphorylated form levels in the FAP-ZF-NPs group compared to the control group. These findings indicate that the magnetocaloric effect can significantly increase the apoptosis of RA- FLS induced by ERS and FAP-ZF-NPs.

An electron microscope was then used to examine the changes in cell state caused by FAP-ZF-NPs. In the control group and the pure AMF group, the structure of mitochondria was observed to be intact, with no injury to the mitochondrial membrane. Upon addition of FAP-ZF-NPs, the mitochondrial structure of RA-FLS was partially altered, swollen, and deformed; the arrangement of mitochondrial cristae was slightly disrupted; some mitochondrial membranes were damaged; and the integrity of the mitochondrial structure was compromised. Endoplasmic reticulum and mitochondrial modifications were pronounced when FAP-ZF-NPs were added following being exposed under the influence of AMF. Indeed, numerous endoplasmic reticulum and mitochondrial structural alterations were observed, with the endoplasmic reticulum being enlarged and swollen, the mitochondrial cristae being disorderedly arranged, and the mitochondrial membrane being severely compromised (Fig. 6E).

As previously discussed, the free radicals induced by FAP-ZF-NPs under the influence of AMF were then detected. Comparatively, to the control group, FAP-ZF-NPs significantly accelerated the oxidative deterioration of RA-FLS cells under AMF conditions (Fig. 6F). It is proposed that FAP-ZF-NPs can considerably increase ROS generation in RA-FLS cells via a magnetocaloric impact. The detection of JC-I demonstrated that the mitochondrial membrane potential of FAP-ZF-NPs was dramatically reduced by the influence of AMF when compared to the control group. In conjunction with the apoptosis detection results, these findings suggest that FAP-ZF-NPs can substantially induce the decline of mitochondrial membrane potential and promote the apoptosis of RA-FLS under AMF conditions (Fig. 6G).

In conclusion, it was believedthat FAP-ZF-NPs can dramatically activate the PERK-ATF4-CHOP and IRE1-XBP1 pathways, as well as enhance mitochondrial damage and ERS in RA-FLS cells in response to AMF, hence promoting synoviocyte apoptosis.

3.7. Therapeutic effects of FAP-ZF-NPs on AIA mice in vivo

Inflammatory synovial hyperplasia and articular cartilage destruction are considered the major pathological processes of RA. These nanoparticles were injected into the joint cavity of AIA mice to assess the effects of FAP-ZF-NPs in the context of RA. Histological staining of mouse joints was performed after 4 weeks of therapy. H&E staining confirmed that synovial tissue was proliferating in the control group, whereas synovial inflammation was observed in the FAP- ZF-NPs treatment group, although to a lesser extent than in the control group.

After applying AMF to mice with AIA, it was discovered that the pure AMF group did not affect synovial tissue and joint inflammation continued to occur in AIA mice. In contrast, FAP-ZF-NPs were shown to drastically reduce synovial tissue inflammation in the presence of AMF (Fig. 7A). The observed findings further elaborated that the joint tissue of AIA mice in the FAP-ZF-NPs + AMF group was well protected with mild synovitis. The cartilage erosion state was studied by TB staining and the results revealed that the control and the pure AMF field group did not exhibit stained cartilage confirming the severe damage of cartilage in these groups. In contrast, the cartilage of AIA mice in the FAP-ZF-NPs treatment group was better stained, and cartilage erosion was negligible; this treatment effect was enhanced by the application of AMF. Through immunohistochemical detection of COL II, it can also be confirmed that FAP-ZF-NPs treatment delayed synovium-induced cartilage damage (Fig. 7B).

In addition, the immunostaining of CD31 showed the decreased formation of synovial vessels after the inhibition of synovium. The observed findings revealed that FAP-ZF-NPs and FAP-ZF-NPs + AMF therapies may considerably decrease synovial tissue proliferation in AIA mice, minimize synovial vessel development, and delay joint destruction (Fig. 7C). Matrix metalloproteinase 3 (MMP3), a common matrix metalloproteinase in synovitis, is the most significant protease responsible for cartilage destruction and an inflammatory marker [43]. It was discovered that FAP-ZF-NPs and FAP-ZF-NPs + AMF treatments could considerably inhibit the production of MMP3 in AIA mice synovial tissue. Therefore, these findings suggest that FAP-ZF-NPs and FAP-ZF-NPs + AMF treatments reduce the synovial invasion and inflammatory expression of cells from RA patients (Fig. 7D).

The effects of FAP-ZF-NPs and AMF on FAP+ cells were further verified in AIA mice. The results demonstrated that the FAP-ZF-NPs group could significantly inhibit the expression of FAP+ cells in AIA mice under the influence of AMF. Fluorescence staining results revealed a significant decrease in the number of positive FAP and VIMENTIN synovial cells in both FAP-ZF- NPs and FAP-ZF-NPs + AMF groups (Fig. 7E). These findings suggest that FAP-ZF- NPs can drastically reduce FAP+ cells in synovial tissue when induced by AMF, indicating a possible beneficial therapeutic influence in reducing AIA mice synovitis.

Finally, the infiltration of synovial macrophages was also evaluated. Previous research has demonstrated that macrophages can respond to external stimuli and polarize into various forms. Some cytokines in synovitis of joints can polarize macrophages in normal synovial tissue, and polarized macrophages primarily include two subtypes: classically activated macrophages (CAMs or M1) and alternatively activated macrophages (AAMs or M2) [44]. M1 macrophages are responsible for the inflammatory response in RA, whereas M2 macrophages play an anti-inflammatory and protective function in promoting inflammation regression. In the development of RA synovitis, RA-FLS interacts with synovial macrophages [28,45]. Therefore; it was verified whether the inhibition of FAP+ FLS had an impact on the polarization of macrophages in the synovium. Fluorescence staining results showed that the number of F4/80 and iNOS double positive cells decreased significantly in the FAP-ZF-NPs and FAP-ZF-NPs + AMF groups (Fig 7F), whereas CD206 did not change considerably. The results demonstrated that the FAP-ZF-NPs group could considerably reduce the infiltration of M1 macrophages in the synovium of AIA mice under the action of AMF, but not synovial M2 macrophages. Therefore, FAP-ZF-NPs were believed to alleviate synovitis by suppressing FAP + cells in synovium, hence indirectly reducing inflammatory macrophage infiltration.

3.8. Treatment evaluation and biosafety assessment

The therapy intervention in this experiment was accomplished using intra-articular injection. By analyzing its expression, it was observed that FAP-ZF-NPs and FAP-ZF-NPs + AMF treatments could significantly reduce the diameter of swollen paws of AIA mice. These findings indicate that FAP-ZF-NPs and FAP-ZF-NPs + AMF treatments reduced systemic inflammation. In addition, the FAP-ZF-NPs group could more significantly inhibit the swollen paw diameter of AIA mice under the action of AMF compared with the ZF-NPs group (Fig.8A) which was also confirmed by clinical scores (Fig.8B). Simultaneously, the expression of serum TNF-α was also investigated in mice of different treatment groups, and the results demonstrated that FAP-ZF-NPs + AMF can significantly inhibit serum inflammation (Fig. 8C). The survival rate and weight changes of AIA mice were monitored during treatment. Throughout the entire treatment period, there were neither fatalities nor the appearance of abnormal symptoms, such as anorexia and anxiety, in mice from any intervention group. The weight in each intervention group increased gradually, following the same patterns as the control group (Fig. 8D). This demonstrates that the current treatment is safe and reliable and that it has no effect on the metabolic biophysical parameters of mice. Histological staining revealed no evident histopathological abnormalities or lesions in the internal organs of mice in either the treatment or control
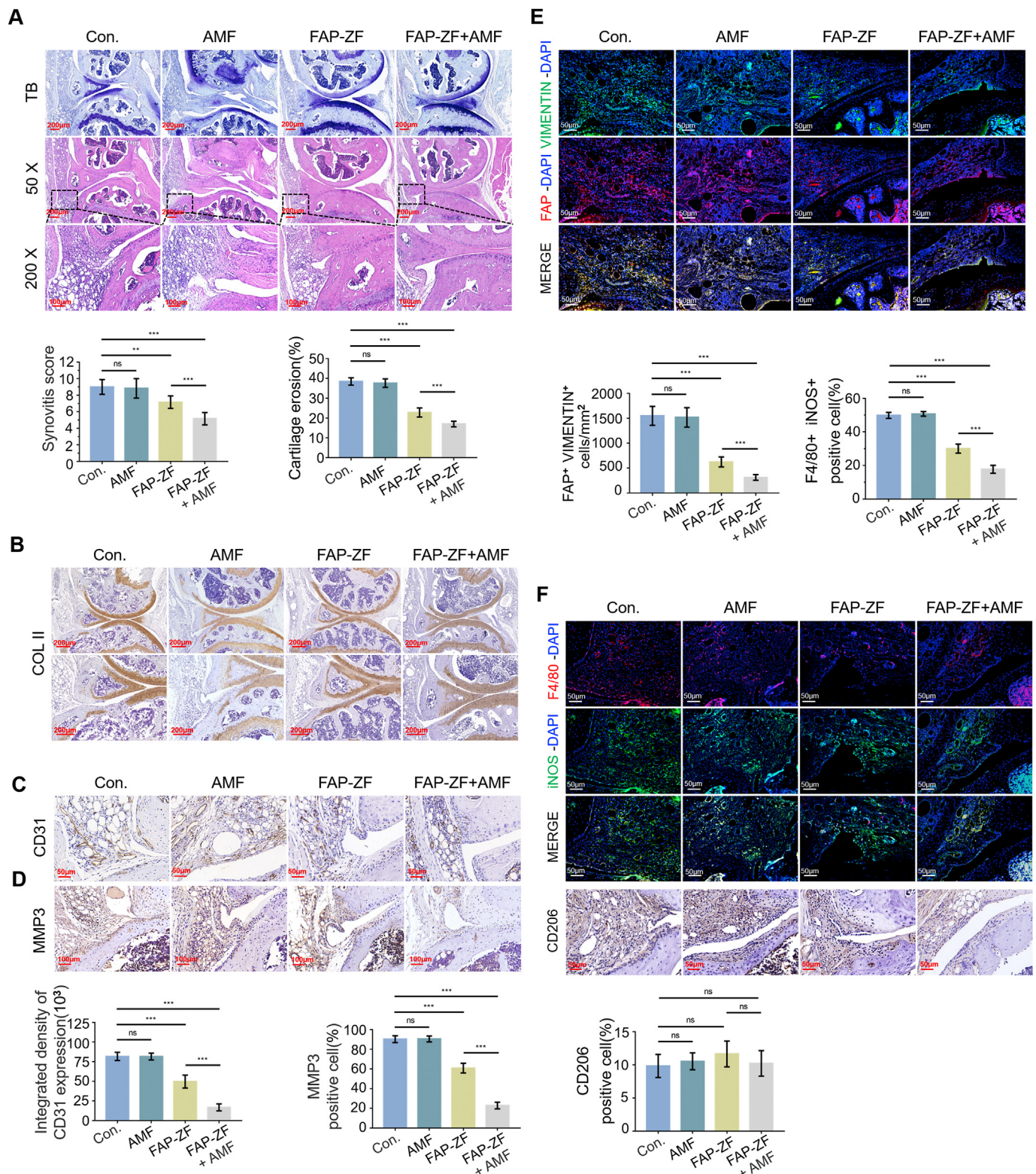
Fig. 7. Therapeutic effects of FAP-ZF-NPs on AIA mice in vivo (A) Representative images of H&E and TB stainings in the synovium of AIA control mice and treatment groups, with quantification of synovitis score (Scale bars, 100 μm or 200 μm). (B) Quantitative analysis of COL II positive cartilage in AIA control mice and treatment groups (Scale bars, 200 μm). (C) Quantitative analysis of CD31 positive synovium in AIA control mice and treatment groups (Scale bars, 50 μm). (D) Representative images of immunohistochemistry of MMP3 in the synovium of AIA control mice and treatment groups (Scale bars, 100 μm). (E) Representative images and quantitative analysis of VIMENTIN in FAP + cells in the synovium of AIA control mice and treatment groups (Scale bars, 50 μm). (F) Representative images and immunofluorescence analysis of F4/80 and iNOS, immunohistochemistry of CD206 in the synovium of AIA control mice and treatment groups. (Scale bars, 50 μm). The data are reported as a mean ± SD and analyzed by one-way ANOVA. n = 6. **$P < 0.05$, ***$P < 0.01$.
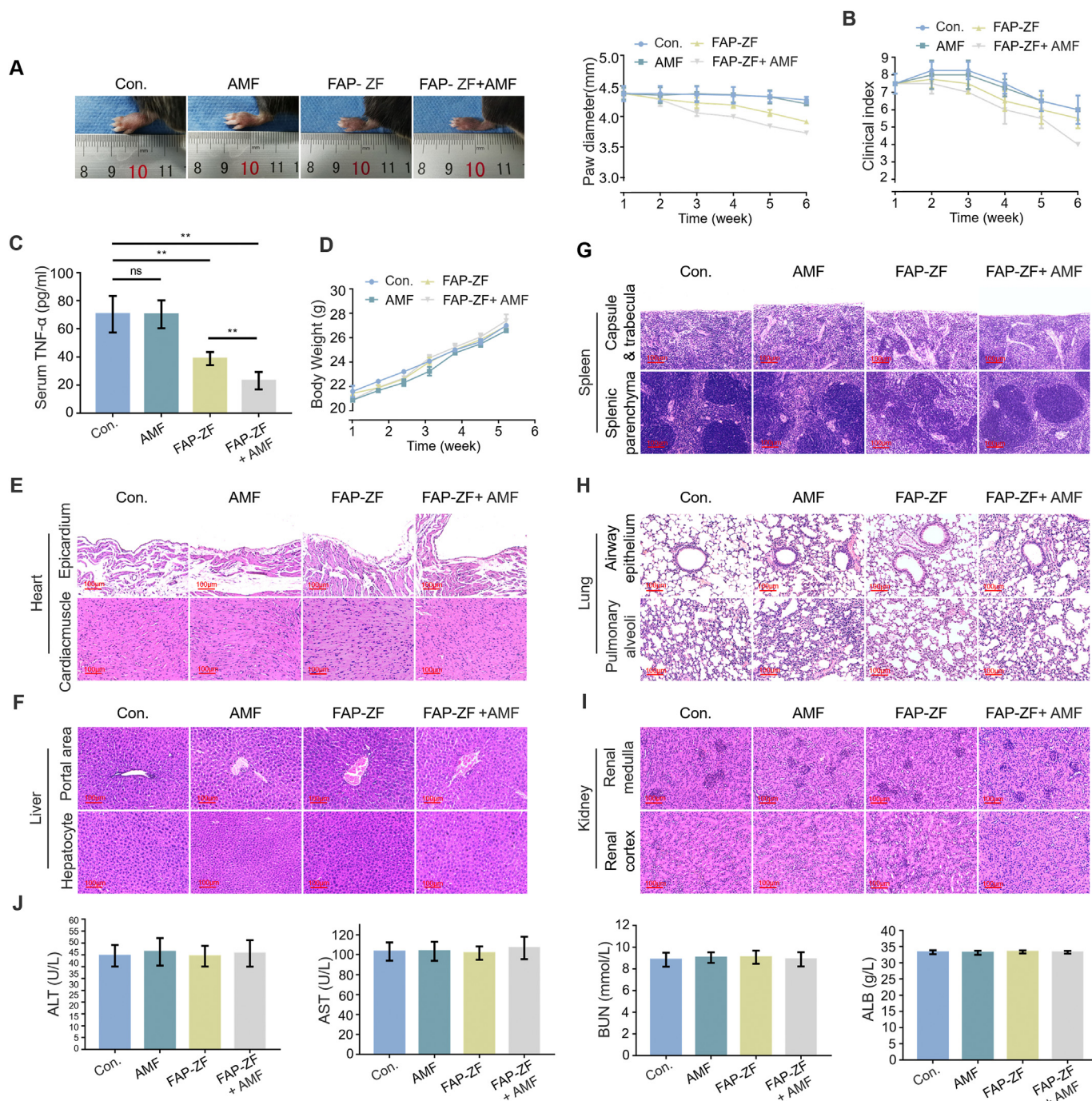
Fig. 8. Treatment evaluation and biosafety assessment (A) Representative images of paws and (B) clinical index of mice after different treatments. (C) Elisa detection of serum TNF-α levels in mice from various treatment groups. (D) Body weight of mice after various treatments. Histopathological analysis of heart (E), liver(F), spleen(G), lung (H), and kidney(I) in mice after different treatments (Scale bars, 100 μm). (J) The blood biochemistry data of mice after different treatments. Data are shown as mean ± SD n = 6. **P < 0.05, ***P < 0.01.

groups. Visceral, heart (Fig. 8E), liver (Fig. 8F), spleen (Fig. 8G), lung (Fig. 8H), and kidney (Fig. 8I) tissues exhibited normal physiological structure and cell morphology. Furthermore, there was no aberrant expression of biochemical indicators such as liver (ALP, AST), kidney (BUN), and serum proteins (ALB) (Fig. 8J). A lateral reaction revealed that there was no damage to the associated metabolic organs during the therapy of intra-articular injection of FAP-ZF-NPs and AMF. According to these findings, no abnormalities were observed in the organs of mice during treatments, demonstrating the feasibility, non-toxicity, and safety profiles of FAP-ZF-NPs injections in the joint cavity.

4. Conclusion

In conclusion, a FAP-targeted ZF-NPs system that can be used alone or in conjunction with AMF to inhibit the progression of RA was developed. This enhanced the protection of articular cartilage and efficiently reduced the process of RA synovitis. This study employed a mechanistic approach to demonstrate that FAP-targeted ZF-NPs exhibited an active delivery function, enabling them to invade RA-FLS in RA synovial tissue and accumulate in the main sites of synovitis. The ingestion of FAP-ZF-NPs in cells was observed to activate the ERS pathway through the PERK-ATF4-CHOP and IRE1-XBP1 pathways. This activation has been

found to result in mitochondrial damage and the induction of apoptosis in RA-FLS. The therapeutic efficacy was further enhanced under the actions of AMF. Furthermore, it was observed that FAP-ZF-NPs did not induce any noteworthy long-term adverse effects in mice. Due to their potent therapeutic action and magnetocaloric therapy, FAP-ZF-NPs have been hypothesized to hold potential as a viable clinical treatment for RA in the future.

CRediT authorship contribution statement

Weizhong Qi: Conceptualization, Writing – original draft. **Li Jin:** Data curation, Software. **Cuixi Wu:** Writing – review & editing. **Hao Liao:** Writing – review & editing. **Mengdi Zhang:** Writing – review & editing. **Zhaohua Zhu:** Validation. **Weiyu Han:** Validation. **Qiyue Chen:** Conceptualization, Project administration, Resources. **Changhai Ding:** Project administration, Resources, Supervision.

Declaration of competing interest

All authors disclosed no relevant relationships.

Data availability

Data will be made available on request.

Acknowledgments

References

[1] H.U. Scherer, T. Haupl, G.R. Burmester, The etiology of rheumatoid arthritis, J. Autoimmun. 110 (2020), 102400, https://doi.org/10.1016/j.jaut.2019.102400.

[2] J.S. Smolen, D. Aletaha, I.B. McInnes, Rheumatoid arthritis, Lancet 388 (10055) (2016) 2023–2038, https://doi.org/10.1016/S0140-6736(16)30173-8.

[3] J.S. Smolen, R. Landewe, F.C. Breedveld, M. Dougados, P. Emery, C. Gaujoux-Viala, S. Gorter, R. Knevel, J. Nam, M. Schoels, D. Aletaha, M. Buch, L. Gossec, T. Huizinga, J.W. Bijlsma, G. Burmester, B. Combe, M. Cutolo, C. Gabay, J. Gomez-Reino, M. Kouloumas, T.K. Kvien, E. Martin-Mola, I. McInnes, K. Pavelka, P. van Riel, M. Scholte, D.L. Scott, T. Sokka, G. Valesini, R. van Vollenhoven, K.L. Winthrop, J. Wong, A. Zink, D. van der Heijde, EULAR recommendations for the management of rheumatoid arthritis with synthetic and biological disease-modifying antirheumatic drugs, Ann. Rheum. Dis. 69 (6) (2010) 964–975, https://doi.org/10.1136/ard.2009.126532.

[4] G.R. Burmester, J.E. Pope, Novel treatment strategies in rheumatoid arthritis, Lancet 389 (10086) (2017) 2338–2348, https://doi.org/10.1016/S0140-6736(17)31491-5.

[5] T. Watanabe, Y. Fujiwara, F.K.L. Chan, Current knowledge on non-steroidal anti-inflammatory drug-induced small-bowel damage: a comprehensive review, J. Gastroenterol. 55 (5) (2020) 481–495, https://doi.org/10.1007/s00535-019-01657-8.

[6] J.C. Wilson, K. Sarsour, S. Gale, A. Petho-Schramm, S.S. Jick, C.R. Meier, Incidence and risk of glucocorticoid-associated adverse effects in patients with rheumatoid arthritis, Arthritis Care Res. 71 (4) (2019) 498–511, https://doi.org/10.1002/acr.23611.

[7] S. Obeid, P. Libby, E. Husni, Q. Wang, L.M. Wisniewski, D.A. Davey, K.E. Wolski, F. Xia, W. Bao, C. Walker, F. Ruschitzka, S.E. Nissen, T.F. Luscher, Cardiorenal risk of celecoxib compared with naproxen or ibuprofen in arthritis patients: insights from the PRECISION trial, Eur Heart J Cardiovasc Pharmacother 8 (6) (2022) 611–621, https://doi.org/10.1093/ehjcvp/pvac015.

[8] J.U. Scher, C. Ubeda, A. Artacho, M. Attur, S. Isaac, S.M. Reddy, S. Marmon, A. Neimann, S. Brusca, T. Patel, J. Manasson, E.G. Pamer, D.R. Littman, S.B. Abramson, Decreased bacterial diversity characterizes the altered gut microbiota in patients with psoriatic arthritis, resembling dysbiosis in inflammatory bowel disease, Arthritis Rheumatol. 67 (1) (2015) 128–139, https://doi.org/10.1002/art.38892.

[9] L. Cai, D. Xu, H. Chen, L. Wang, Y.J.E.R. Zhao, Designing bioactive micro-/nanomotors for engineered regeneration 2 (2021) 109–115.

[10] D. Zhang, W. Li, Y. Shang, L.J.E.R. Shang, Programmable Microfluidic Manipulations for Biomedical Applications, 2022.

[11] W. Xu, S. Jambhulkar, D. Ravichandran, Y. Zhu, M. Kakarla, Q. Nian, B. Azeredo, X. Chen, K. Jin, B. Vernon, D.G. Lott, J.L. Cornella, O. Shefi, G. Miquelard-Garnier, Y. Yang, K. Song, 3D printing-enabled nanoparticle alignment: a review of mechanisms and applications, Small 17 (45) (2021), e2100817, https://doi.org/10.1002/smll.202100817.

[12] S. Sarsaiya, J. Shi, J. Chen, Bioengineering tools for the production of pharmaceuticals: current perspective and future outlook, Bioengineered 10 (1) (2019) 469–492, https://doi.org/10.1080/21655979.2019.1682108.

[13] K.A. Hughes, B. Misra, M. Maghareh, S. Bobbala, Use of stimulatory responsive soft nanoparticles for intracellular drug delivery, Nano Res. 16 (5) (2023) 6974–6990, https://doi.org/10.1007/s12274-022-5267-5.

[14] Y. Zhou, Q. Li, Y. Wu, X. Li, Y. Zhou, Z. Wang, H. Liang, F. Ding, S. Hong, N.F. Steinmetz, H. Cai, Molecularly stimuli-responsive self-assembled peptide nanoparticles for targeted imaging and therapy, ACS Nano 17 (9) (2023) 8004–8025, https://doi.org/10.1021/acsnano.3c01452.

[15] M. Naghdi, M. Ghovvati, N. Rabiee, S. Ahmadi, N. Abbariki, S. Sojdeh, A. Ojaghi, M. Bagherzadeh, O. Akhavan, E. Sharifi, M. Rabiee, M.R. Saeb, K. Bolouri, T.J. Webster, E.N. Zare, A. Zarrabi, Magnetic nanocomposites for biomedical applications, Adv. Colloid Interface Sci. 308 (2022), 102771, https://doi.org/10.1016/j.cis.2022.102771.

[16] Y. Zhu, B. Kong, R. Liu, Y.J.S.M. Zhao, Developing Biomedical Engineering Technologies for Reproductive Medicine, 2022, e20220006.

[17] S. Wang, J. Lv, S. Meng, J. Tang, L. Nie, Recent advances in nanotheranostics for treat-to-target of rheumatoid arthritis, Adv Healthc Mater 9 (6) (2020), e1901541, https://doi.org/10.1002/adhm.201901541.

[18] S.M. Peper, R. Lew, T. Mikuls, M. Brophy, D. Rybin, H. Wu, J. O'Dell, Rheumatoid arthritis treatment after methotrexate: the durability of triple therapy versus etanercept, Arthritis Care Res. 69 (10) (2017) 1467–1472, https://doi.org/10.1002/acr.23255.

[19] J. Li, Q. Meng, Y. Zhang, L. Peng, G. Yu, A.C. Marschilok, L. Wu, D. Su, K.J. Takeuchi, E.S. Takeuchi, Y. Zhu, E.A. Stach, Size-dependent kinetics during non-equilibrium lithiation of nano-sized zinc ferrite, Nat. Commun. 10 (1) (2019) 93, https://doi.org/10.1038/s41467-018-07831-5.

[20] R. Chaudhary, K. Roy, R.K. Kanwar, K. Walder, J.R. Kanwar, Engineered atherosclerosis-specific zinc ferrite nanocomplex-based MRI contrast agents, J. Nanobiotechnol. 14 (2016) 6, https://doi.org/10.1186/s12951-016-0157-1.

[21] C.S. Kumar, F. Mohammad, Magnetic nanomaterials for hyperthermia-based therapy and controlled drug delivery, Adv. Drug Deliv. Rev. 63 (9) (2011) 789–808, https://doi.org/10.1016/j.addr.2011.03.008.

[22] I. Fizesan, C. Iacovita, A. Pop, B. Kiss, R. Dudric, R. Stiufiuc, C.M. Lucaciu, F. Loghin, The effect of Zn-substitution on the morphological, magnetic, cytotoxic, and in vitro hyperthermia properties of polyhedral ferrite magnetic nanoparticles, Pharmaceutics 13 (12) (2021), https://doi.org/10.3390/pharmaceutics13122148.

[23] P. Guo, L. Cui, Y. Wang, M. Lv, B. Wang, X.S. Zhao, Facile synthesis of ZnFe2O4 nanoparticles with tunable magnetic and sensing properties, Langmuir 29 (28) (2013) 8997–9003, https://doi.org/10.1021/la401627x.

[24] N. Higashino, Y.I. Koma, M. Hosono, N. Takase, M. Okamoto, H. Kodaira, M. Nishio, M. Shigeoka, Y. Kakeji, H. Yokozaki, Fibroblast activation protein-positive fibroblasts promote tumor progression through secretion of CCL2 and interleukin-6 in esophageal squamous cell carcinoma, Lab. Invest. 99 (6) (2019) 777–792, https://doi.org/10.1038/s41374-018-0185-6.

[25] T. Zhang, H. Li, J. Shi, S. Li, M. Li, L. Zhang, L. Zheng, D. Zheng, F. Tang, X. Zhang, F. Zhang, X. You, p53 predominantly regulates IL-6 production and suppresses synovial inflammation in fibroblast-like synoviocytes and adjuvant-induced arthritis, Arthritis Res. Ther. 18 (1) (2016) 271, https://doi.org/10.1186/s13075-016-1161-4.

[26] G.S. Firestein, I.B. McInnes, Immunopathogenesis of rheumatoid arthritis, Immunity 46 (2) (2017) 183–196, https://doi.org/10.1016/j.immuni.2017.02.006.

[27] X. Yang, Y. Lin, Y. Shi, B. Li, W. Liu, W. Yin, Y. Dang, Y. Chu, J. Fan, R. He, FAP promotes immunosuppression by cancer-associated fibroblasts in the tumor microenvironment via STAT3-CCL2 signaling, Cancer Res. 76 (14) (2016) 4124–4135, https://doi.org/10.1158/0008-5472.CAN-15-2973.

[28] M.J. Mousavi, E. Farhadi, M. Vodjgani, J. Karami, M.N. Tahmasebi, A. Sharafat Vaziri, M. Asgari, N. Rezaei, S. Mostafaei, A. Jamshidi, M. Mahmoudi, Role of fibroblast activation protein alpha in fibroblast-like synoviocytes of rheumatoid arthritis, Iran. J. Allergy, Asthma Immunol. 20 (3) (2021) 338–349, https://doi.org/10.18502/ijaai.v20i3.6335.

[29] M. Masoumi, M. Bashiri, H. Khorramdelazad, K. Barzaman, N. Hashemi, H.A. Sereshki, A. Sahebkar, J. Karami, Destructive roles of fibroblast-like synoviocytes in chronic inflammation and joint damage in rheumatoid arthritis, Inflammation 44 (2) (2021) 466–479, https://doi.org/10.1007/s10753-020-01371-1.

[30] C. Choi, W. Jeong, B. Ghang, Y. Park, C. Hyun, M. Cho, J. Kim, Cyr61 synthesis is induced by interleukin-6 and promotes migration and invasion of fibroblast-like synoviocytes in rheumatoid arthritis, Arthritis Res. Ther. 22 (1) (2020) 275, https://doi.org/10.1186/s13075-020-02369-8.

[31] Y.H. Yang, E.F. Morand, S.J. Getting, M. Paul-Clark, D.L. Liu, S. Yona, R. Hannon, J.C. Buckingham, M. Perretti, R.J. Flower, Modulation of inflammation and response to dexamethasone by Annexin 1 in antigen-induced arthritis, Arthritis Rheum. 50 (3) (2004) 976–984, https://doi.org/10.1002/art.20201.

[32] B. Bartok, G.S. Firestein, Fibroblast-like synoviocytes: key effector cells in rheumatoid arthritis, Immunol. Rev. 233 (1) (2010) 233–255, https://doi.org/10.1111/j.0105-2896.2009.00859.x.

[33] B.Y. Mo, X.H. Guo, M.R. Yang, F. Liu, X. Bi, Y. Liu, L.K. Fang, X.Q. Luo, J. Wang, J.A. Bellanti, Y.F. Pan, S.G. Zheng, Long non-coding RNA GAPLINC promotes tumor-like biologic behaviors of fibroblast-like synoviocytes as MicroRNA sponging

in rheumatoid arthritis patients, Front. Immunol. 9 (2018) 702, https://doi.org/10.3389/fimmu.2018.00702.

[34] Y. Pang, L. Zhao, T. Meng, W. Xu, Q. Lin, H. Wu, J. Zhang, X. Chen, L. Sun, H. Chen, PET imaging of fibroblast activation protein in various types of cancer using (68)Ga-FAP-2286: comparison with (18)F-fdg and (68)Ga-FAPI-46 in a single-center, prospective study, J. Nucl. Med. 64 (3) (2023) 386–394, https://doi.org/10.2967/jnumed.122.264544.

[35] M. Qi, S. Fan, M. Huang, J. Pan, Y. Li, Q. Miao, W. Lyu, X. Li, L. Deng, S. Qiu, T. Liu, W. Deng, X. Chu, C. Jiang, W. He, L. Xia, Y. Yang, J. Hong, Q. Qi, W. Yin, X. Liu, C. Shi, M. Chen, W. Ye, D. Zhang, Targeting FAPalpha-expressing hepatic stellate cells overcomes resistance to antiangiogenics in colorectal cancer liver metastasis models, J. Clin. Invest. 132 (19) (2022), https://doi.org/10.1172/JCI157399.

[36] R.L. Wiseman, J.S. Mesgarzadeh, L.M. Hendershot, Reshaping endoplasmic reticulum quality control through the unfolded protein response, Mol. Cell. 82 (8) (2022) 1477–1491, https://doi.org/10.1016/j.molcel.2022.03.025.

[37] J.S. Mesgarzadeh, J.N. Buxbaum, R.L. Wiseman, Stress-responsive regulation of extracellular proteostasis, J. Cell Biol. 221 (4) (2022), https://doi.org/10.1083/jcb.202112104.

[38] A.A. Khan, K.S. Allemailem, A. Almatroudi, S.A. Almatroodi, A. Mahzari, M.A. Alsahli, A.H. Rahmani, Endoplasmic reticulum stress provocation by different nanoparticles: an innovative approach to manage the cancer and other common diseases, Molecules 25 (22) (2020), https://doi.org/10.3390/molecules25225336.

[39] B. Li, T. Zhang, M. Tang, Toxicity mechanism of nanomaterials: focus on endoplasmic reticulum stress, Sci. Total Environ. 834 (2022), 155417, https://doi.org/10.1016/j.scitotenv.2022.155417.

[40] L.M. Almeida, B.R. Pinho, M.R. Duchen, J.M.A. Oliveira, The PERKs of mitochondria protection during stress: insights for PERK modulation in neurodegenerative and metabolic diseases, Biol. Rev. Camb. Phil. Soc. 97 (5) (2022) 1737–1748, https://doi.org/10.1111/brv.12860.

[41] J.E. Chipuk, G.P. McStay, A. Bharti, T. Kuwana, C.J. Clarke, L.J. Siskind, L.M. Obeid, D.R. Green, Sphingolipid metabolism cooperates with BAK and BAX to promote the mitochondrial pathway of apoptosis, Cell 148 (5) (2012) 988–1000, https://doi.org/10.1016/j.cell.2012.01.038.

[42] H. Rottenberg, J.B. Hoek, The path from mitochondrial ROS to aging runs through the mitochondrial permeability transition pore, Aging Cell 16 (5) (2017) 943–955, https://doi.org/10.1111/acel.12650.

[43] C.B. Carballo, Y. Nakagawa, I. Sekiya, S.A. Rodeo, Basic science of articular cartilage, Clin. Sports Med. 36 (3) (2017) 413–425, https://doi.org/10.1016/j.csm.2017.02.001.

[44] S. Tardito, G. Martinelli, S. Soldano, S. Paolino, G. Pacini, M. Patane, E. Alessandri, V. Smith, M. Cutolo, Macrophage M1/M2 polarization and rheumatoid arthritis: a systematic review, Autoimmun. Rev. 18 (11) (2019), 102397, https://doi.org/10.1016/j.autrev.2019.102397.

[45] A.P. Croft, J. Campos, K. Jansen, J.D. Turner, J. Marshall, M. Attar, L. Savary, C. Wehmeyer, A.J. Naylor, S. Kemble, J. Begum, K. Durholz, H. Perlman, F. Barone, H.M. McGettrick, D.T. Fearon, K. Wei, S. Raychaudhuri, I. Korsunsky, M.B. Brenner, M. Coles, S.N. Sansom, A. Filer, C.D. Buckley, Distinct fibroblast subsets drive inflammation and damage in arthritis, Nature 570 (7760) (2019) 246–251, https://doi.org/10.1038/s41586-019-1263-7.